Optical detection of transverse spin-Seebeck effect in permalloy film using Sagnac interferometer microscopy

Ryan McLaughlin, Dali Sun, Chuang Zhang, Matthew Groesbeck, and Z. Valy Vardeny

Phys. Rev. B **95**, 180401 — Published 8 May 2017

DOI: 10.1103/PhysRevB.95.180401

Optical Detection of Transverse Spin-Seebeck effect in Permalloy Film using Sagnac Interferometer Microscopy

Ryan McLaughlin[†], Dali Sun[†,‡], Chuang Zhang, Matthew Groesbeck, Z. Valy Vardeny*

Department of Physics & Astronomy, University of Utah, Salt Lake City, Utah, 84112, USA

Abstract

Macroscopic spatially spin distribution caused by the application of an in-plane thermal gradient in a conducting ferromagnetic film, known as transverse spin-Seebeck effect (TSSE), is in many cases overshadowed by thermoelectric and magneto-thermoelectric effects when using the conventional electrical detection via the inverse spin Hall effect. Here we report an optical method for the detection and characterization of TSSE response in permalloy films using magneto-optical Kerr effect with an ultrasensitive fiber-optic Sagnac interferometer microscope that is free of magneto-thermoelectric artefacts, which also allows measurements with field direction parallel and perpendicular to the film surface. We found a substantial anisotropy in the permalloy TSSE coefficient, where the 'in-plane magnetization' coefficient is much larger than that in the 'out-of-plane magnetization'.

†These authors contributed equally to this work.

*To whom correspondence should be addressed: val@physics.utah.edu

‡Current address: Department of Physics, North Carolina State University, Raleigh, NC, 27695, USA

The young field of 'Spin Caloritronics' seeks to exploit the strong coupling between spin currents and heat currents with application opportunities in novel devices [1,2]. It has been shown that a temperature gradient in a ferromagnetic (FM) metal [3,4] and alloys [5], FM semiconductor [6,7], or FM insulator [8-14] in the presence of a magnetic field $\boldsymbol{B}$ spontaneously generates a position-dependent accumulation of spin-polarized carriers that forms spin current ($\boldsymbol{J}_S$) in an adjacent non-magnetic overlayer; this was dubbed the spin-Seebeck effect (SSE) [2]. The SSE has been shown to exist even in the paramagnetic phase above the FM phase-transition temperature in some cases [15,16]. Among the spin caloritronics processes, longitudinal SSE response (LSSE, where $\boldsymbol{J}_S$ is parallel to the direction of thermal gradient) in magnetic insulators have been extensively studied [9-14], whereas attempts to measure the transverse SSE response (TSSE, where $\boldsymbol{J}_S$ is perpendicular to the direction of thermal gradient) [3,6-8] have raised a number of questions [17-21]. In particular, the steady state TSSE in conducting FM films has not been thoroughly explored.

So far the SSE has been exclusively detected by depositing onto the FM film a "spin-detection layer" that consists of a non-magnetic metal (NM) having strong spin-orbit coupling (SOC) such as Pt, which converts the spin current in the FM layer into charge current in the NM overlayer via the inverse spin Hall effect (ISHE) [3]. We note, however that the ISHE voltage that is used to detect the SSE in the FM substrate is quite small (of the order of several μV/K) and phenomenologically similar to a number of thermoelectric and magneto-thermoelectric artefacts such as the regular Seebeck effect, the proximity/anomalous/planar Nernst effect and the LSSE induced by an unintentional out-of-plane thermal gradient [17-21]. Therefore it has been a major experimental obstacle to separate these artefact voltages from the SSE-related ISHE voltage, and this has led to debates in the literature for some years.

In principle, optical spectroscopy such as micro-Brillouin light scattering (BLS) offers an elegant non-contact measurement method for investigating the spatial difference between the thermally activated magnon and phonon populations in a magnetic system [22,23], which is considered to be the underlying mechanism accounting for the SSE (dubbed 'phonon-magnon drag' effect) [24-28]. However, the present BLS resolution for sensing magnon/phonon temperature difference that results from a limited thermal gradient in the FM still cannot provide direct evidence in support of this model [22,23].

In contrast, the magneto-optic Kerr effect (MOKE) has been systematically used in the past years for measuring spin accumulation in semiconductors [29,30] and metals [31]. This has been achieved using three different typical configurations, namely longitudinal, polar and transverse MOKE, depending on the magnetization direction respect to the probe beam's plane of incident (see Supplementary Material Fig. S1 [32]). In these measurements the Kerr rotation angle is proportional to the material magnetization [33], and thus is a function of the spin accumulation. It therefore seems reasonable that a spatially-resolved MOKE method may be used to measure SSE with more confidence than employing electrical detection via ISHE of a NM overlayer, which is prone to thermoelectric and magneto-thermoelectric artefacts.

We note that another type of spin-related Seebeck effect, namely the longitudinal spin-*dependent* Seebeck effect (SDSE) [2,34] has been reported using time-resolved MOKE in the picosecond time domain in a nanoscale sample size [35,36]. The SDSE is described in terms of spin-dependent single-particle effects [2], and thus the generated spin accumulation is limited to the spin diffusion length of carriers (several nm) at the edge of FM metal; consequently the SDSE is usually measured in a nanoscale spin-valve configuration [2,34,35]. In contrast, the SSE relies on the interaction between conduction electrons and long-range coherent excitations such as

magnons and phonons, and therefore the spatially distribution of spin accumulation may extend over several millimeters [24]. The use of MOKE to detect the steady state TSSE over a macroscopic length scale (several mm) of FM metal has so far remained elusive.

In this work we report a CW optical detection study of TSSE in the FM metal permalloy (NiFe), which is conceptually close to the original TSSE report [3]. For these measurements we have used a modified fiber Sagnac interferometer based on the design conceived by J. Xia et al. [37], having a Kerr rotation angle resolution of ~20 nanoRadians (nRad) and spatial resolution of ~1.3 μm (Supplementary Material Fig. S2 [32]). A quick estimation reveals that in this case the magnon temperature resolution may reach ~0.05 Kelvin, which is two orders of sensitivity higher than in conventional MOKE and BLS methods [22,23]. For the TSSE measurements, the Sagnac interferometer was adapted into a 2D scanning confocal microscope with a diffraction-limited spot size of ~1 μm and a maximum image size of 25 mm × 25 mm [Figs. 1(a) and (b)]. The samples investigated were 50 nm thick (2mm × 5mm) NiFe thin films grown by e-beam deposition on clean silicon nitride (SiN)/Si, sapphire, or gadolinium gallium garnet (GGG) substrates, capped by 100 nm SiO_2 overlayer to prevent oxidation. The samples were connected to two copper blocks with a separation of 4 mm using thermally conductive glue. The temperatures of the two copper blocks were independently controlled using separate heaters, while the temperature gradient, ΔT (applied parallel to the NiFe film) was monitored by a thermal IR imaging camera (Fig. 1(c) and Supplementary Material Fig. S3 [32]). An image of the Kerr rotation angle of the NiFe film shows a homogenous magnetization **M** throughout the entire strip (Supplementary Material Fig. S4 [32]). The sample was exposed to a DC magnetic field (B = 150 mT) of which direction was set to be out-of-plane to probe polar MOKE effect ($TSSE_{PM}$, $\boldsymbol{B}\perp\Delta\boldsymbol{T}$) and in-plane to probe longitudinal MOKE effect ($TSSE_{LM}$, $\boldsymbol{B}\parallel\Delta\boldsymbol{T}$) (these MOKE

configurations are shown in Fig. 1). The corresponding *M-B* loops in these two configurations have been measured by the Sagnac interferometer at room temperature, as shown in Fig. 1(d).

Figure 2 shows a typical change in Kerr rotation angle, Δθ measured in the 'polar configuration' ($TSSE_{PM}$) of a NiFe/sapphire sample. We note that the NiFe magnetization, $\boldsymbol{M}$ is aligned along the out-of-plane direction when $B > 150$ mT (see Fig. 1(d)). Under $TSSE_{PM}$ configuration, the conventional electrical ISHE method is inapplicable since the spin current, $\boldsymbol{J_S}$ is generated along the spin polarization direction ($V_{ISHE} = 0$), $\boldsymbol{S}$; whereas MOKE can still measure the obtained TSSE because it measures spin accumulation and thus is not affected by the $\boldsymbol{M} \| \boldsymbol{J_S}$ configuration.

Using the thermal imaging camera we observed that the temperature-controlled sample holder comes to thermal equilibrium in a time period of about 20 minutes. In order to confirm that the observed rise (fall) in Kerr rotation angle, Δθ on the cold (hot) side of the NiFe strip is directly related to the temperature rather than a slow drift in the interferometer, the Sagnac beam was fixed at the hot (cold) end of the NiFe strip and Δθ vs. heating time, t [namely Δθ(t)] was measured continuously while one of the Cu blocks was heated. Figure 2(a) shows Δθ(t) at the left side of the NiFe strip. When the left side of the NiFe strip was heated (namely $T_L > T_R$), then Δθ(t) at the hot end dropped with approximately the same time constant as that of the temperature rise, until it stabilized. Similarly, when the Sagnac beam was fixed at the cold end, Δθ(t) is clearly reversed to that at the hot end [Fig. 2(b)]. The decrease of Δθ(t) at the hot end is expected since the magnetization in a FM, M(T) decreases with temperature, *T*. In contrast, *Δθ(t) increase* at the cold end is surprising; since the 'cold end' actually is maintained at room temperature by a copper heat sink and thus no Δθ should have been obtained. Therefore Δθ increase at the cold end suggests that there is an additional 'dynamic steady-state' Kerr rotation angle response that

originates from the in-plane thermal gradient when the NiFe slab is not in thermal equilibrium; this is exactly the behavior expected from *TSSE response in the conducting FM film*. Paramagnetic SSE from the GGG substrate [16] is unlikely to explain our data because it usually occurs at cryogenic temperatures (below 20K) and under high magnetic field (~9 Tesla). The contribution of paramagnetic SSE in our limited field range and at room temperature should be below the resolution of our detection apparatus.

We also confirmed that $\Delta\theta$ polarity at each end of the NiFe strip is reversed when the direction of either the magnetic field vector or the temperature gradient vector is reversed [Figs. 2(c) and 2(d)]. This is consistent with previous reports of TSSE measured by electrical means [3-7]. We note that the obtained $\Delta\theta$ is in the range of 200 to 500 nrad, indicating that a high-sensitivity Sagnac interferometer is *necessary* for measuring such a subtle $\Delta\theta$ angle. As another control experiment, a 20 nm thick gold film was deposited on a Sapphire substrate, and the same measurements were performed. We found no $\Delta\theta$ in the Kerr rotation angle for the non-magnetic Au strip (Supplementary Material Fig. S5 [32]). Also possible 'bending' of the FM magnetization that leads to the formation of an out-of-plane magnetization component generated with in-plane thermal gradient can also be ruled out for our measurement (see Supplementary Material Fig. S6 [32]).

Figures 3(a) and 3(b) show $\Delta\theta(x)$ as a function of the position, x along the NiFe film deposited on three different substrates; in both '$TSSE_{PM}$' and '$TSSE_{LM}$' configurations (see Supplementary Material section 4 and Fig. S4 [32]). The obtained $\Delta\theta(x)$ profile on each substrate explicitly exhibits the typical decrease at the hot end but clear *increase* at the cold end of the film when applying ΔT along the positive $\boldsymbol{x}$ direction (i.e. $T_L<T_R$), or vice versa when applying ΔT in the

opposite direction. Also we note that $\Delta\theta(x)$ profile is nearly linear, indicating a well-accepted signature of the TSSE response [2-8]. In addition, when the entire strip was heated uniformly (i.e. ΔT=0), only a monotonic decrease of the magnetization, *independent* of the position, x on the NiFe strip was observed (Supplementary Material Fig. S9 [32]). We can also rule out other possible SSE (or SDSE) processes (e.g. longitudinal SSE/SDSE along in-plane thermal gradient, or unintentional out-of-plane thermal gradient [20,21]) (see discussion related to Supplementary Material Figs. S10-S12 [32]).

The origin of the TSSE process is generally explained by a phenomenological model dubbed 'phonon-magnon drag spin dynamics' [7,24-28]. In this model, the thermally activated non-equilibrium phonons propagate through the entire insulator substrate causing a steady state lattice temperature gradient in the FM overlayer, which, in turn modulates the spatial distribution of its magnons density via the magnon-phonon interaction. Consequently the cone angle of the non-equilibrium magnetization precession at temperature T_m decreases (increases) at the hot (cold) end of the FM film compared to that under equilibrium conditions at temperature T_P (see Fig. 4(a)), where T_m and T_p are the magnon and phonon (or lattice) temperature, respectively. This is accompanied by a flow of balancing spin current that diffuses towards (away from) the hot (cold) end of FM/NM (say Pt) interface, which, if electrical detection is used results in a linear asymmetrical spatial dependence of the ISHE signal in the Pt overlayer [4]. If the Sagnac MOKE only senses the magnetization distribution in the NiFe film (represented by the $T_m(x)$ profile), then according to the 'phonon-magnon drag' model the measured $T_m(x)$ slope should be similar or slightly smaller than that of the phonon temperature profile $T_p(x)$, similar to that inferred using the BLS method [22,23]. However this is opposite to what we observed in Figs. 4b and 4c. The measured magnon temperature profile (dubbed here as the effective magnon temperature, $T_m^*(x)$)

shows a *larger slope* compared to that of the T_P profile, suggesting an additional contribution of spin accumulation ($\pm\Delta\theta_{TSSE}$) to the Kerr response at each end of the NiFe strip.

In order to more accurately determine the TSSE coefficient that relates $\Delta\theta(x)$ to the temperature gradient ΔT, we focus on the application of a small temperature gradient, namely ΔT=[T(hot)-T(cold)] ~1K, in which the reduced magnetization from the direct average heating is minimized, and therefore the increased Kerr angle at the cold end can be clearly identified (Supplementary Material Figs. S7 and S8 [32]). Under these conditions the obtained $\Delta\theta(x)$ profile can be described by the following $\Delta\theta(x)$ profile relation:

$$\Delta\theta(\mathrm{x}) = \theta(\mathrm{x}) - \theta_0(\mathrm{x}) = -\mathrm{K_T}(\mathrm{T_P}(\mathrm{x}) - \mathrm{T_0}) + \mathrm{G_{KS}}(\mathrm{T_p}(\mathrm{x}) - \mathrm{T_m}(\mathrm{x})) = \theta_\mathrm{T}(\mathrm{x}) + \Delta\theta_{\mathrm{TSSE}}(\mathrm{x}) \equiv -\mathrm{K_T}(\mathrm{T_m^*}(\mathrm{x}) - \mathrm{T_0}); \quad (1)$$

$$G_{KS}(T_p(x) - T_m(x)) \equiv S_K \, {dT_P}/{dx}; \quad (2)$$

In Eq. (1) $\mathrm{K_T}$ is a coefficient that describes the change in Kerr rotation angle with a homogeneous change in temperature (without the added contribution from SSE-induced spin accumulation), and $\mathrm{T_0}$ and $\theta_0(\mathrm{x})$ are the ambient temperature and Kerr angle with no heat applied to the sample. For simplicity, G_{KS} is a *product* that includes the spin-to-Kerr conversion factor, magnon-phonon interaction, and spin accumulation coefficient due to the difference between the temperatures of the phonon and magnon systems, $T_p(x) - T_m(x)$ [38]. $T_m^*(x)$ is defined as the calculated effective magnon temperature which is normalized by the coefficient, K_T (here $T_m^*(x)$ including the added contribution from SSE-induced spin accumulation).

We first measured K_T separately for the NiFe film deposited on the three used substrates in both 'polar' and 'longitudinal' MOKE configurations, when the entire NiFe strip was heated uniformly (Supplementary Material Fig. S9 [32]). $T_m^*(x)$ in Eq. (1) is shown in the left y-axis of all panels in Fig. 3. The decrease of T_m^* at the cold (left) end corresponds to the increase of $\Delta\theta$ in the right y-axis when applying ΔT along +x direction (red plots in Fig. 3). $T_p(x)$ in Eq. (1) is recorded by the thermal IR imaging camera. However, the actual maximum difference between T_p and T_m in the NiFe film may be in the range of hundreds of μ-Kelvin only at the very ends of FM film according to the theoretical calculation [27], which may cause the value of actual 'G_{KS}' to be extraordinarily large. We note that the spin accumulation increases linearly with the applied temperature gradient ($\propto \nabla T$) [4,38]. Therefore, in analogy to the traditional spin Seebeck coefficient by electrical ISHE detection ($V_{ISHE}/\Delta T$), here we define the optical spin Seebeck coefficient as: $\Delta\theta_{TSSE} \equiv S_K \, {dT_P}/{dx}$ (Eq. 2), where S_K can be derived experimentally. From all the temperature profiles we obtained S_K in both $TSSE_{PM}$, S_K^P and $TSSE_{LM}$, S_K^L for the three substrates used, as summarized in Table I. The observed miniature increased Kerr rotation angle that originates from such a small ΔT shows that the Sagnac MOKE measurement is indeed an essential sensitive tool for detecting the TSSE response directly (without the necessity of a Pt 'spin detector' overlayer).

We note that S_K shows a strong dependence on the choice of substrate and direction of the applied magnetic field (see Table I). In particular S_K^L in NiFe/sapphire structure is larger than that in NiFe/SiN, in agreement with TSSE measured via electrical detection in previous reports [4]. Interestingly, S_K^L is larger compared to S_K^P in NiFe film deposited on all three substrates. Such S_K

anisotropy has not been observed before, since the conventional electrical detection based on ISHE is not viable in the '$TSSE_{PM}$' configuration.

The different obtained S_K values for NiFe deposited on three different substrates support the phonon-mediated TSSE model, and rule out the possibility of a mechanism such as SDSE that is intrinsic to the FM metal that does not rely on magnon-phonon interaction (see detailed discussion in Supplementary Material Figs. S10-12 [32]). As shown in Table I, S_K^L is correlated with the thermal conductivity of the substrates ($\sigma_{thermal}$), and is also influenced by the acoustic-impedance mismatch (or Kapitza resistance) at the interface between the substrate and NiFe overlayer ([4], see Supplementary Material section 10 [32]).

The obtained anisotropy of the TSSE coefficient in the NiFe film, namely $S_K^P < S_K^L$ has not been observed before (see Supplementary Material section 10 [32]). We believe that it originates from the anisotropic coupling between phonons and magnons in the two NiFe magnetization configurations. This is supported by the BLS spectra of magnons in the NiFe film (Table I and Supplementary Material Fig. S14 [32]). In the $TSSE_{PM}$ configuration, the magnon frequency, ν_m is ~4 to 5 GHz, whereas in the $TSSE_{LM}$ configuration ν_m is much higher ~10 to 12 GHz; and this difference indicates different coupling strengths with the substrate's phonons.

In summary, we demonstrate a successful steady state magneto-optical detection method for studying the intrinsic TSSE in a single isolated FM layer, without resorting to additional non-magnetic layers for detecting spin accumulation. We show the first observation of *transverse* SSE response, which might solve the controversial question of whether or not a true TSSE exists in metallic FM films.

Acknowledgements: RM and CZ were supported by the Utah NSF-Material Science & Engineering Center (DMR-1121252); DS was supported by the NSF DMR-1404634; MG was supported by the MURI-AFOSR FA9550-14-1-0037.

References:

1. H. Ohno, Nat. Mater. **9**, 952 (2010).
2. G. Bauer, E. Saitoh, and B. J. van Wees, Nat. Mater. **7**, 885 (2012).
3. K. Uchida, S. Takahashi, K. Harii, J. Ieda, W. Koshibae, K. Ando, S. Maekawa, and E. Saitoh, Nature **455**, 778 (2008).
4. K. Uchida, H. Adachi, T. An, T. Ota, M. Toda, B. Hillebrands, S. Maekawa, and E. Saitoh, Nat. Mater. 10, 737 (2011).
5. S. Bosu, Y. Sakuraba, K. Uchida, K. Saito, T. Ota, E. Saitoh, and K. Takanashi, Phys. Rev. B **83**, 224401 (2011).
6. C. M. Jaworski, J. Yang, S. Mack, D. D. Awschalom, J. P. Heremans, and R. C. Myers, Nat. Mater. **9**, 898 (2010).
7. C. M. Jaworski, J. Yang, S. MacK, D. D. Awschalom, R. C. Myers, and J. P. Heremans, Phys. Rev. Lett. **106**, 186601 (2011).
8. K. Uchida, J. Xiao, H. Adachi, J. Ohe, S. Takahashi, J. Ieda, T. Ota, Y. Kajiwara, H. Umezawa, H. Kawai, G. E. W. Bauer, S. Maekawa, and E. Saitoh, Nat. Mater. **9**, 894 (2010).
9. K. Uchida, H. Adachi, T. Ota, H. Nakayama, S. Maekawa and E. Saitoh. Appl. Phys. Lett. **97**, 172505 (2010).
10. A. Kirihara, K. Uchida, Y. Kajiwara, M. Ishida, Y. Nakamura, T. Manako, E. Saitoh, and S. Yorozu, Nat. Mater. **11**, 686 (2012).

11. T. Kikkawa, K. Uchida, Y. Shiomi, Z. Qiu, D. Hou, D. Tian, H. Nakayama, X. F. Jin, and E. Saitoh, Phys. Rev. Lett. **110**, 067207 (2013).
12. K. Uchida, M. Ishida, T. Kikkawa, a Kirihara, T. Murakami, and E. Saitoh, J. Phys. Condens. Matter **26**, 343202 (2014).
13. G. Siegel, M. C. Prestgard, S. Teng, and A. Tiwari, Sci. Rep. **4**, 4429 (2014).
14. M. Agrawal, V. I. Vasyuchka, A. A. Serga, A. Kirihara, P. Pirro, T. Langner, M. B. Jungfleisch, a. V. Chumak, E. T. Papaioannou, and B. Hillebrands, Phys. Rev. B **89**, 224414 (2014).
15. C. M. Jaworski, R. C. Myers, E. Johnston-Halperin, and J. P. Heremans, Nature **487**, 210 (2012).
16. S. M. Wu, J. E. Pearson, and A. Bhattacharya, Phys. Rev. Lett. **114**, 186602 (2015).
17. A. D. Avery, M. R. Pufall, and B. L. Zink, Phys. Rev. Lett. **109**, 196602 (2012).
18. M. Schmid, S. Srichandan, D. Meier, T. Kuschel, J. M. Schmalhorst, M. Vogel, G. Reiss, C. Strunk, and C. H. Back, Phys. Rev. Lett. **111**, 187201 (2013).
19. I. V. Soldatov, N. Panarina, C. Hess, L. Schultz, and R. Schäfer. Phys. Rev. B **90**, 104423 (2014).
20. D. Meier, D. Reinhardt, M. Schmid, C. H. Back, J.-M. Schmalhorst, T. Kuschel, and G. Reiss. Phys. Rev. B 88, 184425 (2013).
21. D. Meier, D. Reinhardt, M. van Straaten, C. Klewe, M. Althammer, M. Schreier, S. T. B. Goennenwein, A. Gupta, M. Schmid, C. H. Back, J,-M. Schmalhorst, T. Kuschel and G. Reiss, Nat. Commun. 6, 8211 (2015).
22. D. R. Birt, K. An, A. Weathers, L. Shi, M. Tsoi and X. Li. Appl. Phys. Lett. **102**, 082401 (2013).

23. M. Agrawal, V. I. Vasyuchka, A. A. Serga, A. D. Karenowska, G. A. Melkov, and B. Hillebrands. Phys. Rev. Lett. **111**, 107204 (2013).

24. J. Xiao, G. E. W. Bauer, K. C. Uchida, E. Saitoh, and S. Maekawa, Phys. Rev. B **81**, 214418 (2010).

25. H. Adachi, K. I. Uchida, E. Saitoh, J. I. Ohe, S. Takahashi, and S. Maekawa, Appl. Phys. Lett. **97**, 252506 (2010).

26. H. Adachi, K. Uchida, E. Saitoh, and S. Maekawa. Rep. Prog. Phys. **76**, 036501 (2013).

27. M. Schreier, A. Kamra, M. Weiler, J. Xiao, G. E. W. Bauer, R. Gross, and S. T. B. Goennenwein. Phys. Rev. B **88**, 094410 (2013).

28. S. M. Rezende, R. L. Rodríguez-Suárez, R. O. Cunha, A. R. Rodrigues, F. L. A. Machado, G. A. Fonseca Guerra, J. C. Lopez Ortiz, and A. Azevedo, Phys. Rev. B **89**, 014416 (2014).

29. Y. K. Kato, R. C. Myers, A. C. Gossard, and D. D. Awschalom, Science **306**, 1910 (2004).

30. S. A. Crooker, M. Furis, X. Lou, C. Adelmann, D. L. Smith, C. J. Palmstrøm, P. A. Crowell. Science, **309**, 2191 (2005)

31. G.-M. Choi and D. G. Cahill, Phys. Rev. B **90**, 214432, 1 (2014).

32. See Supplemental Material at [URL will be inserted by publisher] for the configurations of MOKE measurements; sensitivity of Sagnac Interferometer; temperature profile on three substrates; 'A-B' method; absence of TSSE-related MOKE signal in Au strip; control experiment for refuting 'out of plane' magnetization; analysis of the MOKE response upon heating; Kerr rotation sensitivities (Kerr vs. T); discussion on the different spin-Seebeck effect and its MOKE measurement techniques; TSSE coefficient.

33. P. N. Argyres, Phys. Rev. **97**, 334 (1955).

34. A. Slachter, F. L. Bakker, J-P. Adam and B. J. van Wees Nat. Phys. **6**, 879-882 (2010).

35. G.-M. Choi, C.-H. Moon, B.-C. Min, K.-J. Lee and D. G. Cahill. Nat. Phys. **11**, 576-581 (2015).

36. J. Kimling, G.-M. Choi, J. T. Brangham, T. Matalla-Wagner, T. Huebner, T. Kuschel, F. Yang and D. G. Cahill. arXiv: 1608.00702.

37. J. Xia, P. T. Beyersdorf, M. M. Fejer, and A. Kapitulnik, Appl. Phys. Lett. **89**, 062508 (2006).

38. K. Uchida, T. Ota, H. Adachi, J. Xiao, T. Nonaka, Y. Kajiwara, G. E. W. Bauer, S. Maekawa, and E. Saitoh. J. Appl. Phys. **111**, 103903 (2012).

39. C. J. Glassbrenner and G. A. Slack, Phys. Rev. **134**, A1058 (1964).

40. N. L. Hecht, D. E. Mccullum, and G. G. A, Ceram. Eng. Sci. Proc. **9**, 1313 (1988).

41. M. Faheem and K. Lynn, Am. J. Anal. Chem. **5**, 695 (2014).

42. R. Berman, E. L. Foster, and J. M. Ziman, Proc. R. Soc. London. Ser. A. Math. Phys. Sci. 237, 344 (1956).

Figures and captions

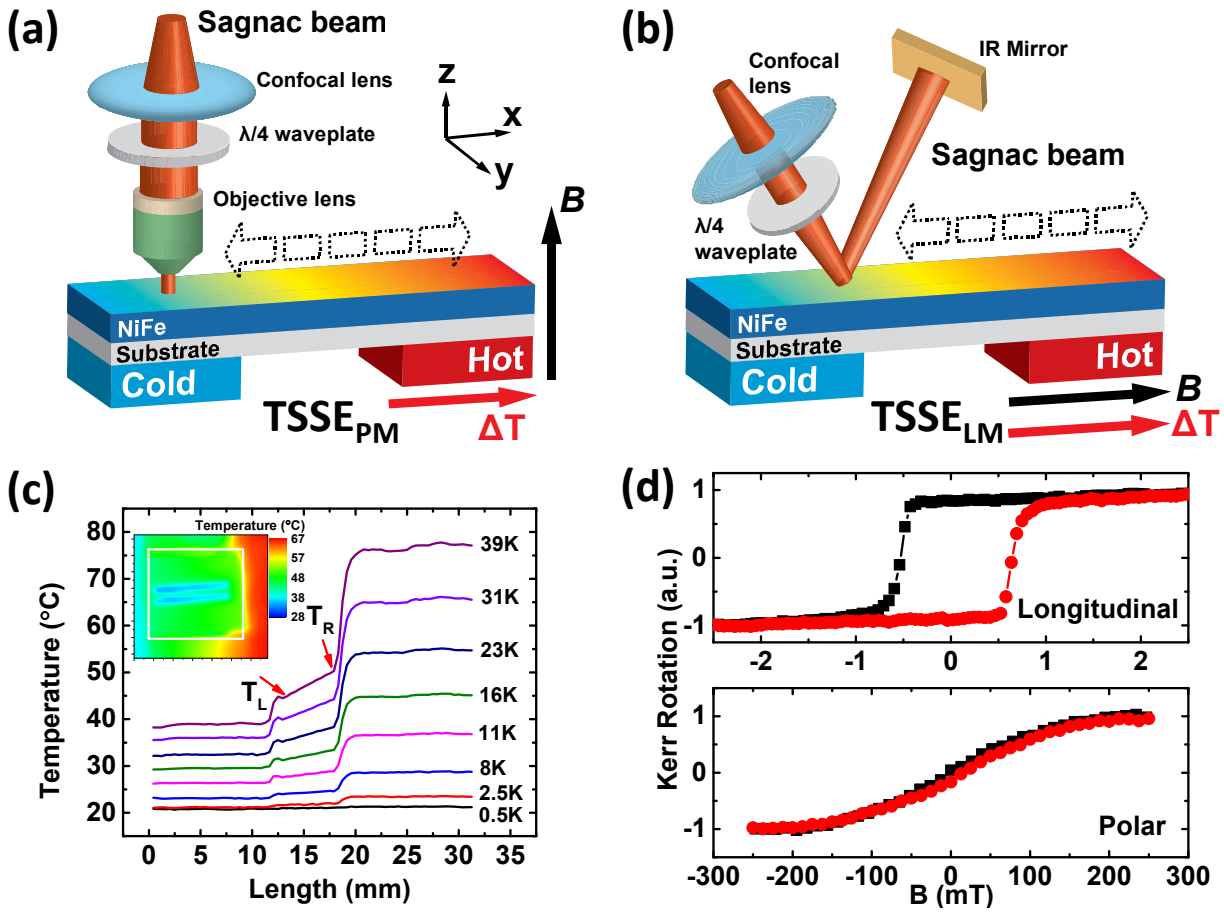

FIG. 1. (Color online) (a) and (b) Schematic illustration of the Sagnac set-up for $TSSE_{PM}$ and $TSSE_{LM}$ measurement, respectively. (c) The obtained temperature profiles in NiFe/sapphire as a function of ΔT (denoted on the right). The inset shows an image of the actual temperature profile. The substrate with NiFe films (blue strips) on top is sketched by a white square. (d) *M*-*B* loops of a NiFe/sapphire measured in 'longitudinal' and 'polar' MOKE configurations (see Supplementary Material Fig. S1 [32]).

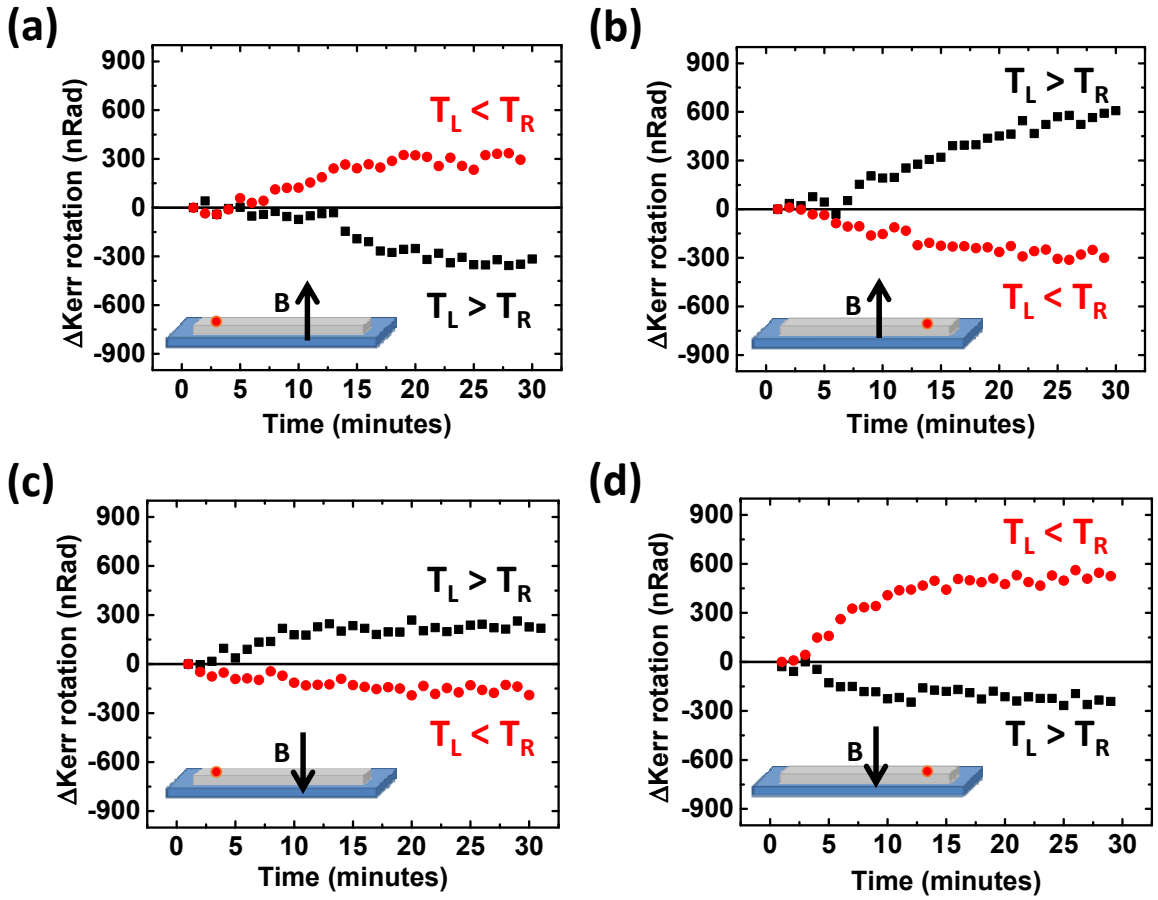

FIG. 2. (Color online): Time evolution of the TSSE-related Kerr rotation angle in a NiFe strip deposited on GGG substrate subjected to a temperature gradient of 0.2K/mm. The insets show schematically the measurement geometry where the position of the Sagnac laser spot (red circle) and orientation of the magnetic field vector (black arrow) are denoted. The DC magnetic field is fixed at B= 150 mT.

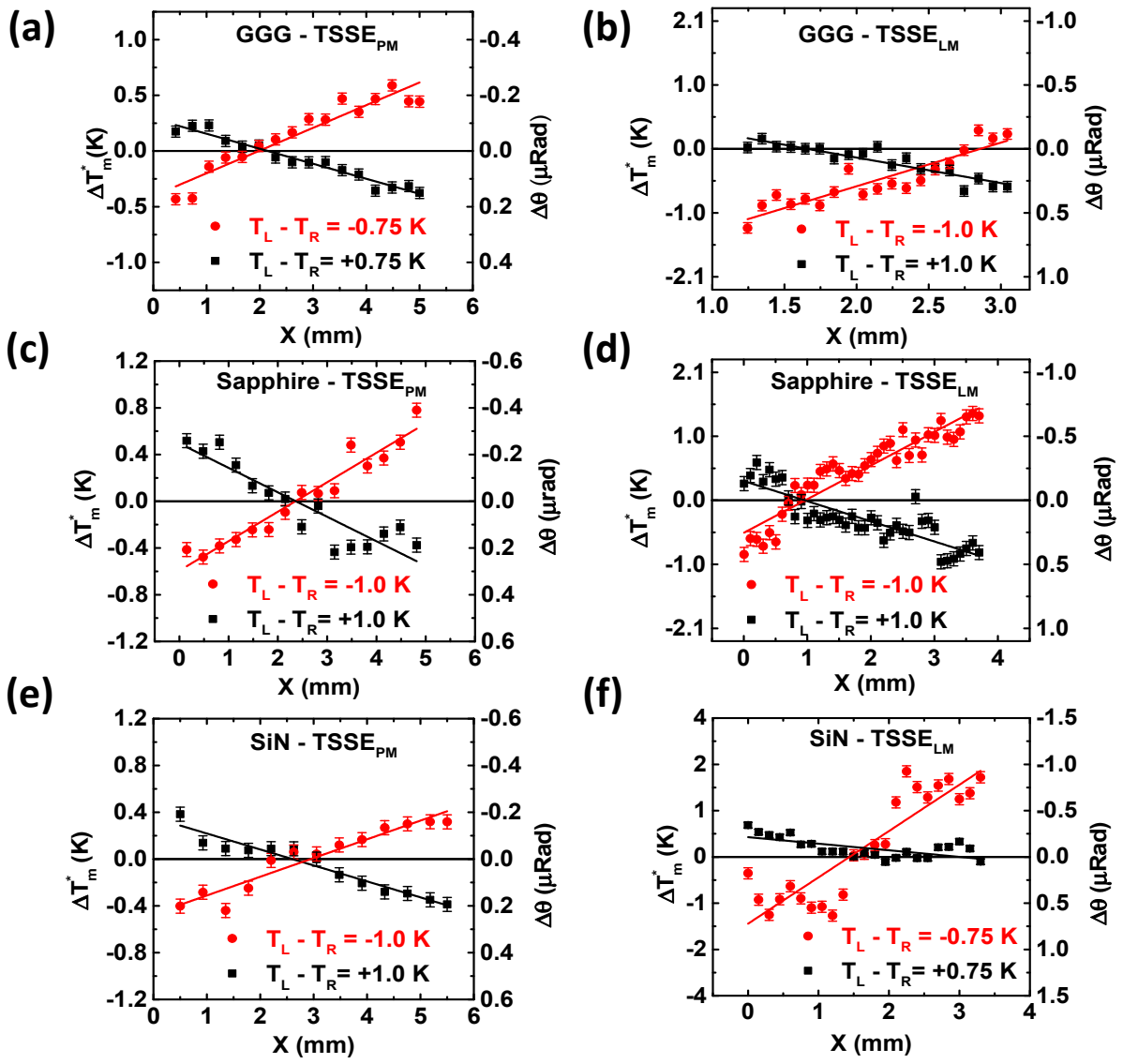

FIG. 3. (Color online): The profile of the TSSE-related Kerr angle, Δθ(*x*) (right y-axis) and the corresponding profile of T_m^*(x) (left y-axis) measured in NiFe strips on three different substrates GGG (a-b), sapphire (c-d), and SiN (e-f), in both 'TSSE$_{PM}$' and 'TSSE$_{LM}$' configurations having different ΔT (=T_L-T_R) as denoted. The Kerr angle changes are plotted vs. *x* as measured under thermal equilibrium conditions (~30 minutes after the heating was turned on, see Fig. 2), at field value that saturates the NiFe magnetization.

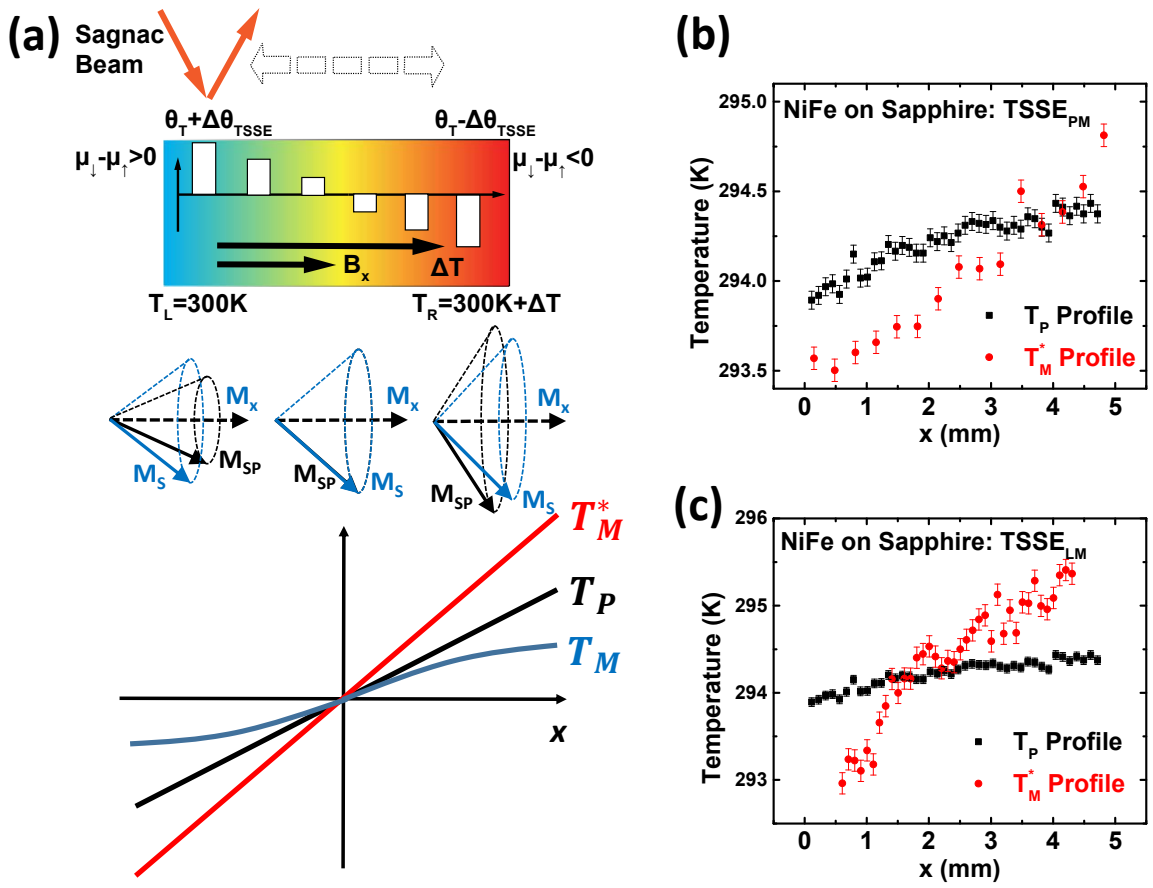

FIG. 4. (Color online): (a) *Top panel*: Illustration of opposite spin accumulation ($\mu_{\uparrow}$-$\mu_{\downarrow}$) that is formed at each end of a NiFe strip when ΔT is applied in the $\boldsymbol{x}$ direction. *Middle panel*: the cone precession angle of the magnetization vector as a function of $\boldsymbol{x}$ formed upon the temperature gradient, where M_{SP} (black arrows) and M_S (blue arrows) represent the equilibrium magnetization at T_P and the actual non-equilibrium magnetization at T_m. *Bottom panel*: the three temperature profiles (not to scale) in a heated FM metal film; T_P, T_m and T_m^*. (b) and (c) The obtained T_P and T_m^* profile (as denoted) measured in NiFe/sapphire structure by thermal camera and MOKE, respectively in the '$TSSE_{PM}$' and '$TSSE_{LM}$' configuration.

	NiFe on GGG	On Sapphire	On SiN
$TSSE_{PM}$ (nRad·K^{-1})	90 ± 20	190 ± 30	290 ± 25
$TSSE_{LM}$ (nRad·K^{-1})	1,080 ± 90	970 ± 65	490 ± 95
PM-Kerr vs T (nRad·K^{-1})	-410 ± 50	-510 ± 50	-500± 50
LM-Kerr vs T (nRad·K^{-1})	-450 ± 50	-680 ± 50	-420 ± 50
BLS frequency (PM) (GHz)	4.6, 13.2	4.0, 16.2	4.9
BLS frequency (LM) (GHz)	10.2	10.7, 20.2	10.5
Substrate $\sigma_{thermal}$(W·m^{-1}·K^{-1})	7.5[41]	25[42]	135 for Si[39]; 2 to 5 for SiN[40]

Table I. The obtained optical SSE coefficients $TSSE_{PM}$ (S_K^P) and $TSSE_{LM}$ (S_K^L), Kerr rotation sensitivities (Kerr vs. T), BLS magnon frequencies in two configurations, and thermal conductivities for GGG, sapphire, and SiN substrates.